Available online at www.sciencedirect.com
ScienceDirect
Journal of Photochemistry and Photobiology A: Chemistry 187 (2007) 1–9
Journal of Photochemistry and Photobiology A:Chemistry
www.elsevier.com/locate/jphotochem

Spectroscopy and kinetics of the gas phase addition complex of atomic chlorine with dimethyl sulfoxide

K.M. Kleissas [a,1], J.M. Nicovich [a], P.H. Wine [a,b,*]

[a] School of Chemistry and Biochemistry, Georgia Institute of Technology, Atlanta, GA 30332-0400, United States
[b] School of Earth and Atmospheric Sciences, Georgia Institute of Technology, Atlanta, GA 30332-0340, United States

Received 5 July 2006; received in revised form 4 August 2006; accepted 4 August 2006
Available online 1 September 2006

Abstract

Time-resolved UV–vis absorption spectroscopy has been coupled with 248 nm laser flash photolysis of Cl_2CO in the presence of $CH_3S(O)CH_3$ (and in some cases O_2, NO, or NO_2) to generate the $CH_3(Cl)S(O)CH_3$ radical adduct in the gas phase and study the spectroscopy and kinetics of this species at 296 K. $CH_3(Cl)S(O)CH_3$ is found to possess a strong absorption band with $\lambda_{max} = 394$ nm and $\sigma_{max} = (4.0 \pm 1.4) \times 10^{-17}$ cm^2 molecule^{-1} (base e); the gas phase spectrum of $CH_3(Cl)S(O)CH_3$ is very similar to previously reported liquid phase spectra in chloroalkane and water solvents. Reaction of $CH_3(Cl)S(O)CH_3$ with O_2 is found to be very slow, and our data suggest that the rate coefficient for this reaction is less than 3×10^{-18} cm^3 molecule^{-1} s^{-1}. Rate coefficients for $CH_3(Cl)S(O)CH_3$ reactions with $CH_3(Cl)S(O)CH_3$ (k_3), NO (k_9), and NO_2 (k_{10}) in units of 10^{-11} cm^3 molecule^{-1} s^{-1} are found to be $2k_3 = 6.0 \pm 2.4$, $k_9 = 1.2 \pm 0.3$, and $k_{10} = 2.1 \pm 0.3$, where the uncertainties are estimates of accuracy at the 95% confidence level.

Keywords: DMSO; Sulfur chemistry; Atmospheric chemistry; Radical spectroscoopy; 3-Electron bond

1. Introduction

The gas phase reaction of atomic chlorine with dimethyl sulfoxide (DMSO; $CH_3S(O)CH_3$) is of interest in atmospheric chemistry [1] and, as a result, has been the focus of a number of publications [2–7]. Nicovich et al. have recently employed the laser flash photolysis (LFP) – resonance fluorescence technique to study the temperature and pressure dependences of the Cl + DMSO rate coefficient [7]; these investigators used their results in conjunction with earlier results obtained in low-pressure flow reactors [4,5] to show that reaction occurs via both H-abstraction and addition pathways:

$$Cl + CH_3S(O)CH_3 \rightarrow HCl + CH_3S(O)CH_2 \quad (1a)$$

$$Cl + CH_3S(O)CH_3 + M \rightarrow CH_3(Cl)S(O)CH_3 + M \quad (1b)$$

At room temperature and atmospheric pressure, the reported rate coefficient is nearly gas kinetic, with the addition pathway accounting for $87 \pm 2\%$ of the overall reactivity [7]. Electronic structure calculations support the existence of an adduct with a Cl–S bond strength of approximately 70 kJ mol^{-1} [6,7], and a recent experimental determination [7] based on observation of the decay of laser-flash-generated Cl into equilibrium with a Cl reservoir (presumably $CH_3(Cl)S(O)CH_3$), reports an adduct bond strength in good agreement with the theoretical results. In the molecular orbital picture, the ground electronic state of $CH_3(Cl)S(O)CH_3$ is characterized by an S–Cl three-electron bond containing two bonding σ electrons and one antibonding σ^* electron [8,9]. Although $CH_3(Cl)S(O)CH_3$ has not been directly observed in the gas phase, a transient absorption feature with $\lambda_{max} \sim 400$ nm that is assigned to this species has been observed in the liquid phase in both chloroalkane [8,10] and H_2O [9,11] solvents.

In this paper we report the results of an experimental study of the gas phase Cl + DMSO reaction that couples LFP with time-resolved UV–vis absorption spectroscopy (TRUVVAS). The gas phase absorption spectrum of $CH_3(Cl)S(O)CH_3$ (including absolute absorption cross-sections) is reported for the first

* Corresponding author at: School of Earth and Atmospheric Sciences, Georgia Institute of Technology, Atlanta, GA 30332-0340, United States.
E-mail address: paul.wine@chemistry.gatech.edu (P.H. Wine).
[1] Present address: Merck & Co., Inc., WP78-110, PO Box 4, West Point, PA 19486-0004, United States.

1010-6030/$ – see front matter © 2006 Elsevier B.V. All rights reserved.
doi:10.1016/j.jphotochem.2006.08.020

time, and the TRUVVAS technique is used as a probe to investigate the kinetics of $CH_3(Cl)S(O)CH_3$ reactions with O_2, NO, and NO_2, and also to get some information about the rates of radical–radical reactions of $CH_3(Cl)S(O)CH_3$. The experimental results are used to evaluate the potential role of $CH_3(Cl)S(O)CH_3$ in atmospheric chemistry. In addition, the experimental results contribute to development of an overall understanding of the kinetics and spectroscopy of gas phase radical + sulfur compound adducts as well as differences (or similarities) between gas and liquid phase spectroscopy and kinetics of these species.

2. Experimental technique

The LFP-TRUVVAS apparatus used in this study is very similar to those we have employed in previous spectroscopic and kinetic studies of $Cl–S(CH_3)_2$ [12] and Cl–SCS [13]. A schematic diagram of the apparatus is published elsewhere [13]. Major elements of the apparatus include a pulsed KrF photolysis laser (248 nm), a 75 W xenon arc lamp cw probe light source, an insulated Pyrex, jacketed reaction cell (100 cm long, 40 mm i.d.), a pre-mixing cell, a monochromator to isolate the probe wavelength, a photomultiplier tube (PMT) to detect the probe radiation, an oscilloscope to record the temporal evolution of the transmitted probe radiation, a computer to store and average the waveforms from the oscilloscope, and numerous optical components to manipulate and align the photolysis and probe beams, which overlapped collinearly as they traversed the length of the reaction cell. Experimental details that are specific to this study are provided below.

All experiments were carried out at room temperature (296 ± 2 K). The $CH_3(Cl)S(O)CH_3$ adduct was generated by 248 nm excimer laser flash photolysis of phosgene (Cl_2CO) in the presence of $CH_3S(O)CH_3$. The absorption cross-section for Cl_2CO at 248 nm is 8.93×10^{-20} cm^2 molecule^{-1} [14] and the photolysis laser fluence ranged from 15 to 45 mJ cm^{-2} pulse^{-1}; the pulse duration was ~25 ns.

All experiments were carried out under "slow flow" conditions, i.e., the linear flow rate of the reaction mixture through the reaction cell (typically 4 cm s^{-1}) was fast enough to replenish the volume of the reaction cell every few laser pulses (the typical laser repetition rate was 0.1 Hz), but slow enough that kinetic observations could be analyzed assuming static conditions.

Concentrations of both $CH_3S(O)CH_3$ and Cl_2CO were measured *in situ* in the slow flow system by UV photometry at 213.9 nm (Zn penray lamp light sources). In units of 10^{-19} cm^2 molecule^{-1}, the cross-sections used to convert 213.9 nm absorbances to concentrations were 53 [15,16] and 1.26 [12] for $CH_3S(O)CH_3$ and Cl_2CO, respectively. Because of its low vapor pressure (0.6 Torr at 298 K [17]), $CH_3S(O)CH_3$ is difficult to handle in the gas phase. The procedure for obtaining reliable concentration measurements in spite of problems with adsorption of $CH_3S(O)CH_3$ on cell walls and windows is discussed in detail elsewhere, as is the procedure for deriving accurate $CH_3S(O)CH_3$ and Cl_2CO concentrations from absorption measurements at a wavelength where both species absorb [7].

In the kinetics experiments, the concentrations of NO and NO_2 were determined from mass flow measurements of NO/N_2 or $NO_2/N_2/O_2$ mixtures combined with photometric measurements of $NO_2/N_2/O_2$ mixtures. The procedure involved first transferring nitric oxide (NO) into a 12L Pyrex bulb and diluting with N_2; pressure measurements provided an estimate of the fraction of NO in the NO/N_2 mixture. At the conclusion of a set of $CH_3(Cl)S(O)CH_3 + NO$ experiments, the NO/N_2 mixture was quantitatively diluted with enough O_2 to convert all NO to NO_2. After allowing several hours for conversion of NO to NO_2, the NO_2 concentration in the mixture was measured by photometry using the 457.9 nm line from an argon ion laser as the light source; the absorption cross-section used to convert measured absorbance to NO_2 concentration was 5.06×10^{-19} cm^2 molecule^{-1} [18]. The NO concentration was determined quantitatively from the measured NO_2 concentration and the known O_2 dilution factor, while the resulting $NO_2/N_2/O_2$ mixture was used for a set of $CH_3(Cl)S(O)CH_3 + NO_2$ experiments. The presence of O_2 in the bath gas in the NO_2 storage bulb prevented slow build up of NO impurity.

The pure gases used in this study were obtained from Air Products (N_2, O_2) and Matheson (Cl_2CO, NO), and had the following stated minimum purities: N_2, 99.999%; O_2, 99.994%; Cl_2CO, 99.0%; NO, 99.0%. The N_2, O_2, and NO were used as supplied. The Cl_2CO was degassed at 77 K prior to use. The liquid DMSO sample had a stated minimum purity of 99.9%. It was transferred into a bubbler fitted with high-vacuum all-Teflon stopcocks, from which it was admitted into the slow flow system entrained in a controlled flow of N_2 bath gas. The bubbler was positioned downstream from the mass flow meter and needle valve that measured and controlled the flow of N_2 into it.

3. Results and discussion

When Cl_2CO was photolyzed in the presence of DMSO, absorption of the UV–vis probe beam was observed throughout the 310–510 nm spectral region. Absorption was observed only when both DMSO and Cl_2CO were simultaneously subjected to LFP. When the photolyzed mixture contained only Cl_2CO, DMSO, and N_2, the observed absorbance (A) decayed slowly with time and, within experimental uncertainty, followed second order kinetics. Under the experimental conditions employed, the appearance of absorbance was always very fast compared to the decay of absorbance. Hence, the peak absorbance for each experiment could be determined with good accuracy by plotting A^{-1} versus time and extrapolating back to $t = 0$ using a linear fit to the A^{-1} versus time data.

3.1. Adduct identification

Evidence verifying the identity of the absorbing species was obtained by measuring its appearance rate. Absorbance temporal profiles were recorded and analyzed using a nonlinear least squares fit to the sum of an exponential rise and an exponential decay (see Fig. 1). In this set of experiments, absorbance disappearance resulted primarily from radical–radical reactions and was not a first-order process. The first-order absorbance

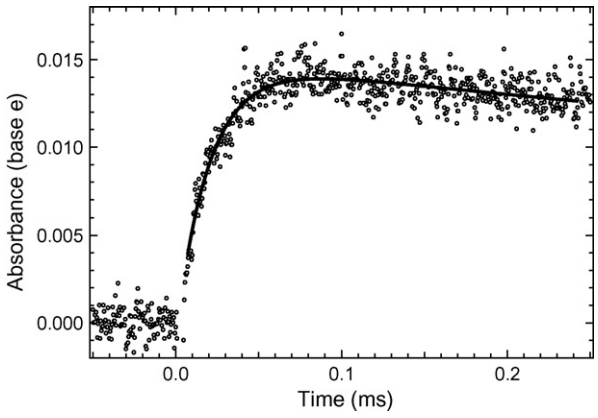

Fig. 1. A typical absorbance (base e) temporal profile observed following laser flash photolysis of $Cl_2CO/DMSO/N_2$ mixtures at $P = 50$ Torr. Concentrations in units of 10^{13} molecules cm^{-3} are $[Cl_2CO] = 158$, $[Cl]_0 \approx 0.5$, and $[DMSO] = 61.1$. The solid line is obtained from a nonlinear least squares fit to the sum of an exponential rise and an exponential decay. The best fit appearance (k_a) and disappearance (k_d) rate coefficients in units of s^{-1} are $k_a = 49{,}600$ and $k_d = 714$.

disappearance rate, k_d, is thus a parameterized rate coefficient rather than the sum of actual loss processes that are quantitatively attributable to specific first order processes. However, because the observed absorbance loss rates are slow compared to the rapid rate of absorbance appearance, the parameterization of the absorbance disappearance as a first order process does not seriously impact the reliability of the analysis to determine the pseudo-first order rate coefficient for absorbance appearance. As exemplified by the data shown in Fig. 1, the quality of the double exponential fits is quite good as long as the fits are limited to a small fraction of the decay. Pseudo-first order appearance rate coefficients (k_a) were measured at a pressure of 50 Torr in N_2 bath gas using a probe wavelength of 390 nm. As shown in Fig. 2, a plot of k_a versus [DMSO] is linear over the range of DMSO concentrations employed. The linearity of the k_a versus [DMSO] plot up to the fastest

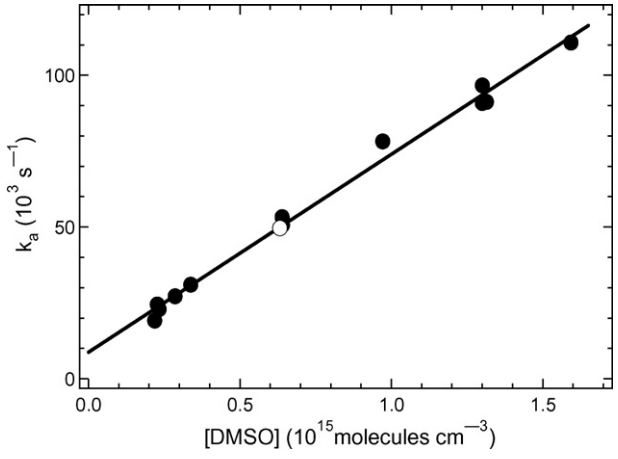

Fig. 2. Plot of k_a vs. [DMSO] for data obtained at $P = 50$ Torr N_2. The solid line is obtained from a linear least squares analysis; its slope gives the second order rate coefficient $k_1 = (6.52 \pm 0.33) \times 10^{-11}$ cm^3 $molecule^{-1}$ s^{-1} where the uncertainty is 2σ and represents precision only. The open circle is the data point obtained from the data shown in Fig. 1.

appearance rate measured (ca. 110,000 s^{-1}) demonstrates that the rate-limiting step in production of the absorbing species is the Cl + DMSO reaction under the conditions investigated. The slope of the k_a versus [DMSO] plot yields the second order rate coefficient $k_1 = (6.52 \pm 0.33) \times 10^{-11}$ cm^3 $molecule^{-1}$ s^{-1} ($k_1 \equiv k_{1a} + k_{1b}$), where the uncertainty is 2σ and represents precision only. The value measured here for k_1(P, T) is in good agreement with the value $(6.34 \pm 0.37) \times 10^{-11}$ cm^3 $molecule^{-1}$ s^{-1} reported at the same temperature and pressure by Nicovich et al. [7] based on measurements of Cl atom decay using atomic resonance fluorescence spectroscopy as the detection technique. The data in Figs. 1 and 2 provide strong evidence that the species being observed is indeed the $CH_3(Cl)S(O)CH_3$ adduct formed from the reaction of Cl with DMSO. Further evidence supporting this assignment comes from comparison of the observed absorption spectrum with reported liquid phase spectra of $CH_3(Cl)S(O)CH_3$ [8,10,11] (see below).

3.2. Adduct absorption spectrum

The absorption spectrum of $CH_3(Cl)S(O)CH_3$ was measured at 100 Torr total pressure in N_2 bath gas. A reference wavelength of 390 nm was selected. Absorption measurements were made at this reference wavelength after every few measurements at other wavelengths. This was done in order to account for systematic drifts in experimental parameters such as laser power, $[Cl_2CO]$, optical alignment, etc. over time. Absorbance measurements at wavelengths other than 390 nm were normalized to the average of the "before" and "after" 390 nm absorbances. The adduct absorption cross-section was carefully measured at 390 nm and all cross-sections were then determined by applying the normalization factor to the carefully measured reference cross-section.

Reagent concentrations employed in the 390 nm cross-section measurements were (in units of 10^{13} molecules cm^{-3}): $[DMSO] \approx 115$; $[Cl_2CO] = 12$–150; $[Cl]_o = 0.05$–0.7. Values for A_0 (defined below) were obtained by extrapolation of A^{-1} versus time (t) data to $t = 0$. Each cross-section measurement involved averaging ~20 photolysis laser pulses. The adduct cross-section at 390 nm (σ_{390}) was determined from the data using the following relationship:

$$\sigma_{390} = \frac{A_0}{l[Cl]_0 F}. \quad \text{(I)}$$

In Eq. (I), A_0 is the absorbance at a time shortly after the laser flash when Cl and $CH_3(Cl)S(O)CH_3$ have reached equilibrium but negligible radical decay has occurred, l is the absorption path length (100 cm), $[Cl]_0$ is the concentration of chlorine atoms produced by the laser flash, and F is the fraction of Cl atoms converted to adduct. As is typical for gas phase spectroscopic data, the absorbance is defined as $A = \ln(I_0/I)$, i.e., it is a base e value.

The parameter F in Eq. (I) can be evaluated from the following relationship:

$$F = (1 - F_1)(1 - F_2)(1 - F_3) \quad \text{(II)}$$

where F_1 is the fraction of Cl atoms that are lost by diffusion from the detection volume and/or reaction with background impurities, F_2 the fraction of Cl atoms that react with DMSO by H-abstraction rather than by addition, and F_3 is the fraction of $Cl + CH_3(Cl)S(O)CH_3$ that exists as Cl when the two species are in equilibrium. Employing high concentrations of DMSO helps to keep F_1 and F_3 small, while employing relatively high total pressure minimizes F_2. Experimental conditions for the cross-section measurements were [DMSO] $\sim 1 \times 10^{15}$ molecules cm^{-3} and N_2 pressure = 300 Torr. Based on the kinetic and thermodynamic data reported by Nicovich et al. [7], we find that $F_2 = 0.15$ and $F_3 = 0.003$ under the above experimental conditions. The background loss rate of Cl atoms (typically found to be $\sim 100\,s^{-1}$ in LFP studies of Cl kinetics that employ resonance fluorescence detection) is probably negligible compared to the pseudo-first order rate coefficient for Cl + DMSO, which is nearly $100{,}000\,s^{-1}$ under the above experimental conditions. However, since the intercept of the plot shown in Fig. 2 is higher than expected based on the known $CH_3(Cl)S(O)CH_3$ unimolecular decomposition rate [7], an unusually fast Cl loss by impurity reactions cannot be completely ruled out. Hence, we conservatively assign F_1 the value 0.05 ± 0.05 to account for all possibilities. The above considerations lead to the result $F = 0.81 \pm 0.06$ where the reported uncertainty is an estimate of accuracy at the 95% confidence level.

Cross-sections obtained from Eq. (I) were found to be independent of $[Cl]_0$ over the range specified above, i.e., Beer's law was obeyed. Evaluation of $[Cl]_0$ required (i) careful measurements of $[Cl_2CO]$ and laser power, (ii) assumption of a quantum yield of 2.0 for production of Cl from 248 nm photolysis of Cl_2CO, and (iii) careful measurements of the photolysis laser beam cross-sectional area and its divergence down the length of the cell (the laser beam area increased by a factor of 1.5 between the cell entrance and exit, and was assumed to be the average of the entrance and exit areas for purposes of evaluating $[Cl]_0$).

The assumption of a quantum yield of 2.0 for Cl atom production from Cl_2CO photolysis is based on strong experimental evidence that, when Cl_2CO is excited at wavelengths in the range 230–260 nm, (a) CO is produced with unit yield [19], (b) the yield of Cl_2 is no more than a few percent [20], and (c) ClCO is not produced with significant yield as a stabilized photo-product [21]. The conclusions that neither Cl_2 nor ClCO are produced with significant yield are based primarily on measurements by Gericke and co-workers of kinetic energy release in the Cl and CO photoproducts; these measurements employed pulsed laser excitation and REMPI-TOFMS detection (REMPI ≡ resonance enhanced multiphoton ionization; TOFMS ≡ time of flight mass spectrometry) [20–22]. It is also worth noting that temperature- and pressure-dependent rate coefficients for ClCO unimolecular decomposition are reported in the literature [23], and are fast enough under the conditions of our experiments that, even if thermalized ClCO were produced via Cl_2CO photolysis, secondary fragmentation would occur on a time scale that is fast compared to the experimental time scale for observation of $CH_3(Cl)S(O)CH_3$ kinetics. Because the Cl_2 yield from Cl_2CO photolysis is so small [20], we do not expect this species to be a significant interference in either the spectroscopic or kinetic studies reported below.

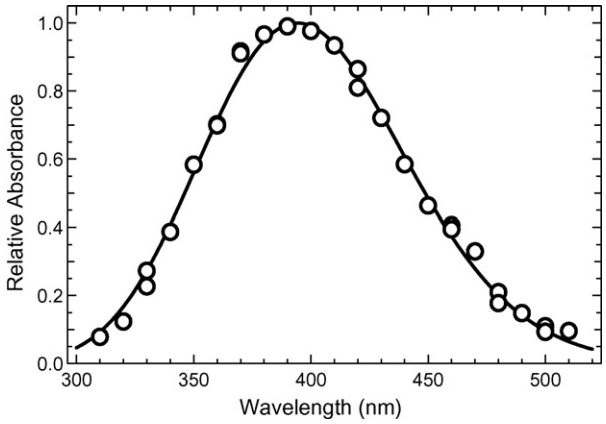

Fig. 3. Absorption spectrum of the $CH_3(Cl)S(O)CH_3$ adduct at a spectral resolution of 3.7 nm.

The $CH_3(Cl)S(O)CH_3$ spectrum measured in this study is shown in Fig. 3. The quarter-meter monochromator used for the measurements had a spectral dispersion of 3.7 nm per mm and slit widths were set at 1.0 mm for all spectral measurements. The expected spectral resolution of 3.7 nm FWHM (full width at half maximum) was confirmed through measurement of the spectra of atomic penray lamp emission lines at several wavelengths within the spectral range of interest. The solid line in Fig. 3 is obtained by fitting absorbance versus wavelength data to a slightly-skewed-Gaussian functional form (see Eq. (III) below); this functional form, which is Gaussian in the limit where $\lambda_{max} - \lambda \ll \lambda_{max}$, has been employed successfully by Ingham et al. to reproduce their measured absorption spectrum for $(CH_3)_2SBr$ [16]. We find that our data are well-described by the slightly-skewed Gaussian function as well, suggesting that the observed absorption spectrum is attributable to a single electronic transition. As mentioned above, the similarity between the gas phase absorption spectrum reported in this study and published liquid phase spectra [8,9,11] lends further support to our conclusion that the species observed in this study is the $CH_3(Cl)S(O)CH_3$ adduct.

Consideration of uncertainties in the parameters that must be known to obtain the adduct cross-section (see above), leads to an estimate of ±35% for the accuracy of the measured cross-section at 390 nm (95% confidence level). We report our measured 390 nm cross-section to be $\sigma_{390} = (4.0 \pm 1.4) \times 10^{-17}$ cm^3 $molecule^{-1}$ s^{-1}. The best fit function (λ in units of nm),

$$\sigma(\lambda) = 4.02 \times 10^{-17} \exp\left\{-41.12\left[\ln\left(\frac{394.1}{\lambda}\right)\right]^2\right\}, \qquad \text{(III)}$$

suggests that maximum absorbance occurs at 394 nm with $\sigma_{max} = 1.01\sigma_{390}$. The absorption cross-section at any desired wavelength in units of cm^2 $molecule^{-1}$ can be obtained with good accuracy using Eq. (III).

In the analysis described above, we ignore the possible occurrence of the following reaction that could potentially convert the H-abstraction product back to Cl (via rapid secondary dissocia-

tion of ClCO):

$$CH_3S(O)CH_2 + Cl_2CO \rightarrow CH_3S(O)CH_2Cl + ClCO \quad (2)$$

The thermochemistry of reaction (2) is highly uncertain, and to our knowledge there is no evidence in the literature supporting the occurrence of this reaction. However, we cannot completely rule out this interfering reaction either. Rapid regeneration of Cl via reaction (2) would increase the parameter F in Eqs. (I) and (II) from 0.81 ± 0.06 to 0.95 ± 0.05. Hence, if a fast rate coefficient for reaction (2) is demonstrated at some time in the future, our reported absorption cross-sections would have to be adjusted downward by a factor of 95/81 = 1.17.

Although Cl_2 absorbs in the wavelength region where we have observed the $CH_3(Cl)S(O)CH_3$ spectrum, we do not believe that there is a significant spectral interference from Cl_2 because (a) as described above, there appears to be little or no photochemical production of Cl_2 and (b) the Cl_2 absorption cross-sections are about two orders of magnitude smaller than those we have measured for $CH_3(Cl)S(O)CH_3$ [24]. Another potential interfering absorber that warrants consideration is $CH_3S(O)Cl$. The results of Riffault et al. [5] and Nicovich et al. [7] suggest that a small fraction of adduct loss (perhaps as much as 10%) could occur via decomposition to $CH_3 + CH_3S(O)Cl$. To our knowledge, the absorption spectrum of $CH_3S(O)Cl$ is unknown. It seems unlikely that $CH_3S(O)Cl$ absorbs strongly enough at $\lambda > 300$ nm to represent a significant interference in this study, particularly since all spectroscopic measurements have been carried out at short times after the photolysis flash where little or no decomposition of $CH_3(Cl)S(O)CH_3$ has occurred.

3.3. Radical–radical reaction kinetics

When reaction mixtures containing only Cl_2CO, DMSO, and N_2 are subjected to 248 nm laser flash photolysis and readily detectable levels of $CH_3(Cl)S(O)CH_3$ are generated, loss of $CH_3(Cl)S(O)CH_3$ is expected to be controlled by radical–radical reactions:

$$CH_3(Cl)S(O)CH_3 + CH_3(Cl)S(O)CH_3 \rightarrow 2CH_3S(O)CH_3 + Cl_2 \quad (3)$$

$$CH_3(Cl)S(O)CH_3 + CH_3S(O)CH_2 \rightarrow CH_3S(O)CH_3 + CH_3S(O)CH_2Cl \quad (4)$$

$$CH_3S(O)CH_2 + CH_3S(O)CH_2 \rightarrow \text{products} \quad (5)$$

$$Cl + CH_3(Cl)S(O)CH_3 \rightarrow CH_3S(O)CH_3 + Cl_2 \quad (6)$$

$$Cl + CH_3S(O)CH_2 \rightarrow \text{products} \quad (7)$$

The Cl self-reaction is very slow and, therefore, is not listed above. If experimental conditions are adopted where $P = 300$ Torr and $[DMSO] > 1 \times 10^{15}$ molecules cm^{-3}, then Cl reacts rapidly to form 85% $CH_3(Cl)S(O)CH_3$ and 15% $CH_3S(O)CH_2$, and dissociation of $CH_3(Cl)S(O)CH_3$ to regenerate Cl is negligibly slow [7]. Under such conditions, reactions (6) and (7) become unimportant. Loss of $CH_3(Cl)S(O)CH_3$ under the specified conditions is expected to be controlled by reactions (3) and (4), while reaction (5) could possibly affect $[CH_3(Cl)S(O)CH_3]$ indirectly by competitively removing $CH_3S(O)CH_2$. Also, as discussed above in the context of the cross-section measurements, the occurrence of reaction (2) could lead to rapid secondary conversion of $CH_3S(O)CH_2$ to $CH_3(Cl)S(O)CH_3$.

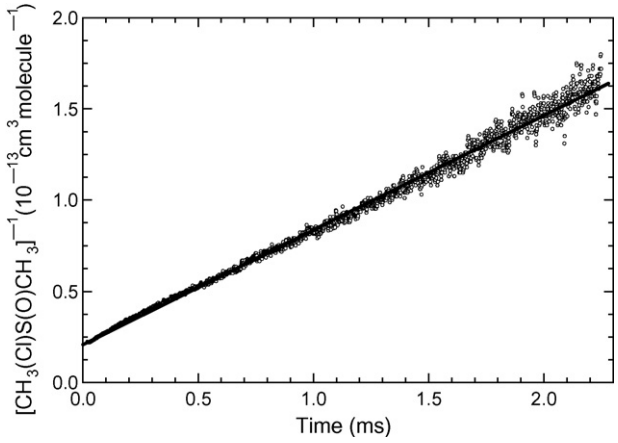

Fig. 4. Typical $CH_3(Cl)S(O)CH_3$ absorbance temporal profile observed following 248 nm laser flash photolysis of Cl_2CO/DMSO/N_2 mixtures. Experimental conditions: $P = 300$ Torr; concentrations in units of 10^{15} molecules cm^{-3} = 12.9 Cl_2CO and 1.82 DMSO. The solid line is obtained from a linear least squares analysis; its slope gives $2k_3 = (6.29 \pm 0.02) \times 10^{-11}$ cm^3 molecule^{-1} s^{-1} under the assumption of scenario (1) described in the text, where the uncertainty is 2σ and represents precision only.

Shown in Fig. 4 is a typical $CH_3(Cl)S(O)CH_3$ temporal profile observed at a monitoring wavelength of 390 nm following 248 nm laser flash photolysis of reaction mixtures containing $(1.5–27) \times 10^{15}$ Cl_2CO per cm^3, $\sim 1.7 \times 10^{15}$ DMSO per cm^3 and 300 Torr N_2. The data are plotted as $[CH_3(Cl)S(O)CH_3]^{-1}$ versus time, so the linearity of the plot indicates that loss of $CH_3(Cl)S(O)CH_3$ (as expected) follows second order kinetics. The concentrations plotted in Fig. 4 are obtained using the value for σ_{390} reported above. The second order rate coefficients obtained from several experiments employing different phosgene concentrations (but constant laser power) are in good agreement, with the mean value obtained for 2 k being 6.65×10^{-11} cm^3 molecule^{-1} s^{-1}. We consider three different scenarios to interpret the measured value for $2k$:

(1) If reactions (2) and (4) are sufficiently slow, then data analyzed in the manner described above and shown in Fig. 4 gives a measurement of $2k_3$.
(2) If reaction (2) is fast enough to rapidly convert $CH_3S(O)CH_2$ back to Cl, then the observed decay is due entirely to reaction (3), but the $CH_3(Cl)S(O)CH_3$ concentration is larger than assumed in our data analysis by a factor of 95/81 as described above in the discussion of potential interference of reaction (2) in the cross-section experiments; hence, the value for $2k_3$ is lower by a factor of 95/81 compared to scenario (1).

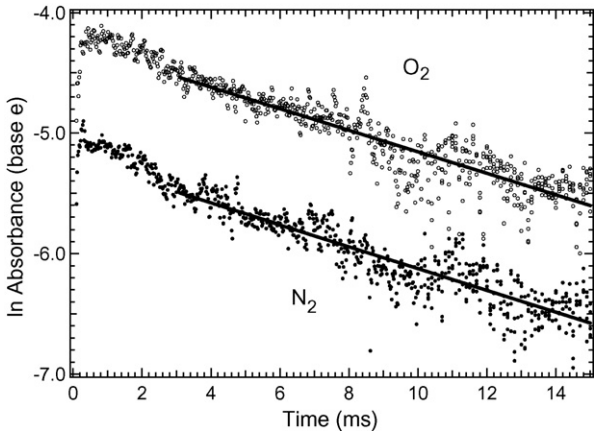

Fig. 5. $CH_3(Cl)S(O)CH_3$ absorbance temporal profiles in N_2 and O_2 plotted as ln A (base e) vs. time. Experimental conditions: $P = 300$ Torr and concentrations in units of 10^{13} molecules cm^{-3} = 47 Cl_2CO, 0.16 Cl_0, and 105 DMSO. The solid lines are obtained from linear least squares analyses of all data at times 3.0–15.0 ms after the laser flash; their slopes give *apparent* pseudo-first order decay rates of $90.5 \pm 3.5\ s^{-1}$ for the N_2 experiment and $89.4 \pm 3.6\ s^{-1}$ for the O_2 experiment (uncertainties are 2σ and represent precision only). For the sake of clarity, the O_2 data are displaced upward on the vertical scale by 1 unit of ln A.

(3) Reaction (2) is negligibly slow, but reaction (4) makes a significant contribution to $CH_3(Cl)S(O)CH_3$ removal. In this case, the true value for $2k_3$ would be smaller than the value derived assuming scenario (1). However, given the observed linearity of the plots (see Fig. 4, for example) and the fact that $[CH_3(Cl)S(O)CH_3] > 5\ [CH_3S(O)CH_2]$ under the experimental conditions employed, it seems highly unlikely that $2k_3$ would be overestimated by more than 15 or 20%.

Based on the above discussion, we choose to report a value for $2k_3$ that is 10% lower than the value obtained by basing the analysis on scenario (1), and we adjust the reported uncertainty to include not only precision and the uncertainty in the absorption cross-section, but also uncertainty that arises because we don't know which of the above three scenarios is correct. This approach leads to the reported value $2k_3 = (6.0 \pm 2.4) \times 10^{-11}$ cm^3 $molecule^{-1}$ s^{-1}.

3.4. Kinetics of the $CH_3(Cl)S(O)CH_3 + O_2$ reaction

To investigate the kinetics of the reaction of $CH_3(Cl)S(O)CH_3$ with O_2,

$$CH_3(Cl)S(O)CH_3 + O_2 \rightarrow \text{ products}, \quad (8)$$

$CH_3(Cl)S(O)CH_3$ absorbance temporal profiles were measured in back-to-back experiments employing N_2 and O_2 or air as the bath gases. The experiments were carried out at 300 Torr total pressure with relatively low $[Cl]_0$ in order to accentuate the importance of any pseudo-first order component in the decay in the presence of O_2. Shown in Fig. 5 are plots of ln A versus time for one set of back-to-back experiments where experimental conditions were held constant except that N_2 and O_2 were interchanged as the bath gas. In both cases, it is clear based on the data and on the analysis discussed above in Section 3.3 that radical–radical reactions make a significant contribution to the observed decays. Nonetheless, the ln A versus time plots are reasonably linear, especially at times more than 3.0 ms after the laser flash. Linear least squares analyses of all data at times 3.0–15.0 ms after the laser flash leads to virtually identical first order decay rates, i.e., $90.5 \pm 3.5\ s^{-1}$ in N_2 bath gas and $89.4 \pm 3.6\ s^{-1}$ in O_2 bath gas (uncertainties are 2σ and represent precision only). The data analysis was restricted to times less than 15 ms after the laser flash because there was so little absorption at later times that a quantitative kinetic analysis was precluded. Reactions (3) and (4), diffusion of $CH_3(Cl)S(O)CH_3$ out of the detection volume, and reaction of $CH_3(Cl)S(O)CH_3$ with background impurities in the bath gases may all contribute to the time evolution of absorbance for the data shown in Fig. 5. However, these data suggest that there is no observable reaction between $CH_3(Cl)S(O)CH_3$ and O_2. In order to put a reasonable upper limit on k_8, however, it is necessary to consider the fact that the secondary chemistry is not identical in N_2 and O_2 bath gases. In O_2, the H-abstraction product $CH_3S(O)CH_2$ is expected to be rapidly converted to a peroxy radical ($CH_3S(O)CH_2OO$) that is almost certainly less reactive toward $CH_3(Cl)S(O)CH_3$ than $CH_3S(O)CH_2$ is. Hence, it is possible (though unlikely) that, in the presence of O_2, some reduction in the rate of loss of $CH_3(Cl)S(O)CH_3$ via reaction (4) is compensated for by a very slow but non-zero rate of reaction of $CH_3(Cl)S(O)CH_3$ with O_2. Taking this complication into account, we conservatively feel that our data supports an upper limit pseudo-first order rate coefficient of $k'_8 < 30\ s^{-1}$ in 300 Torr O_2. This leads to an upper limit bimolecular rate coefficient of $k_8 < 3 \times 10^{-18}$ cm^3 $molecule^{-1}$ s^{-1}.

3.5. Kinetics of $CH_3(Cl)S(O)CH_3$ reactions with NO and NO_2

The reactions of $CH_3(Cl)S(O)CH_3$ with NO and NO_2 were studied at pressures of 30 and 300 Torr in N_2 bath gas. All experiments were carried out under nearly pseudo-first order conditions with $[NO_x]$ in 8- to 60-fold excess over $[CH_3(Cl)S(O)CH_3]$.

$$CH_3(Cl)S(O)CH_3 + NO \rightarrow \text{ products} \quad (9)$$

$$CH_3(Cl)S(O)CH_3 + NO_2 \rightarrow \text{ products} \quad (10)$$

The reagent concentrations in units of 10^{13} molecules cm^{-3} used in these experiments were as follows: $[Cl_2CO] = 50$–650; $[Cl]_0 \sim 0.4$–2; $[DMSO] \approx 105$; $[NO] = 8$–51; $[NO_2] = 6$–45. The DMSO concentration is sufficiently high and the temperature (296 K) sufficiently low that the equilibrium between Cl and $CH_3(Cl)S(O)CH_3$ is driven to well over 99% $CH_3(Cl)S(O)CH_3$ [7]; hence, reactions of Cl with NO and NO_2 have a negligible effect on observed $CH_3(Cl)S(O)CH_3$ kinetics.

As typified by the data shown in Fig. 6, absorbance decays appear exponential, i.e., plots of ln A versus time appear linear, as would be expected if loss of $CH_3(Cl)S(O)CH_3$ is dominated by pseudo-first order reaction with NO_x. However, the peak concentration of $CH_3(Cl)S(O)CH_3$ for the temporal profile shown in Fig. 6, as well as for most other

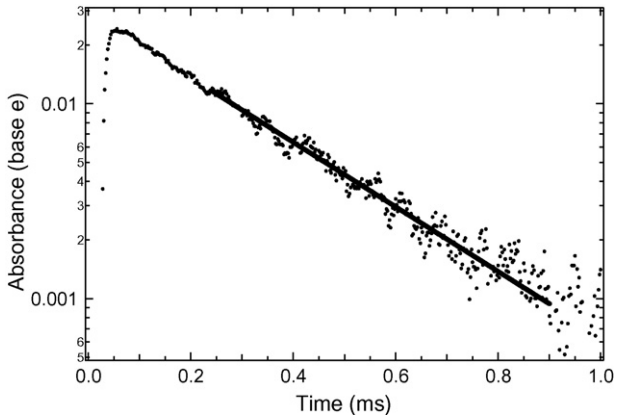

Fig. 6. Typical absorbance (base e) temporal profile observed following 248 nm laser flash photolysis of Cl_2CO/DMSO/NO_x/N_2 mixtures. Experimental conditions: $NO_x = NO_2$; $P = 300$ Torr; concentrations in units of 10^{13} molecules cm^{-3} are [DMSO] = 113, $[Cl_2CO] = 390$, $[Cl]_o \approx 1.0$, and $[NO_2] = 18.3$. The solid line is obtained from a linear least squares analysis of the $\ln A$ vs. time data using only data where $A < 0.012$; its slope gives the pseudo-first order decay rate $k' = 3810 \pm 80\ s^{-1}$ where the uncertainty is 2σ and represents precision only.

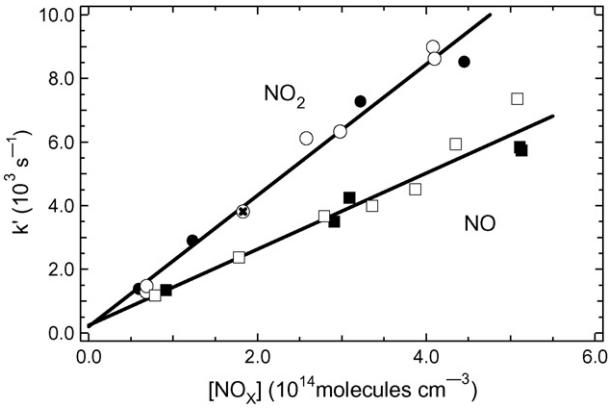

Fig. 7. Plots of pseudo-first-order adduct decay rate (k') vs. [NO_x] for data obtained at pressures of 30 and 300 Torr N_2. Circles are NO_2 data points and squares are NO data points. Filled symbols are 30 Torr data and open symbols are 300 Torr data; the open symbol with an "×" in the middle is the data point obtained from the temporal profile shown in Fig. 6. Solid lines are obtained from linear least-squares analyses of all NO and NO_2 data, respectively; their slopes give the following bimolecular rate coefficients in units of 10^{-11} cm^3 $molecule^{-1}$ s^{-1}: $k_9 = 1.20 \pm 0.19$ and $k_{10} = 2.06 \pm 0.18$; uncertainties are 2σ and represent precision only.

temporal profiles measured, is large enough for reactions (3) and (4) to make small but significant contributions to $CH_3(Cl)S(O)CH_3$ removal. As a result, pseudo-first order decay rates were obtained from the slopes of plots like the one shown in Fig. 6 using only data obtained at times where $A < 0.012$ (i.e., $[CH_3(Cl)S(O)CH_3] < 4 \times 10^{12}$ per cm^3). Based on the discussion of radical–radical reaction kinetics in Section 3.3 above, we consider the contribution of reactions (3) and (4) to $CH_3(Cl)S(O)CH_3$ removal to be insignificant when $[CH_3(Cl)S(O)CH_3] < 4 \times 10^{12}$ per cm^3.

Measured pseudo-first order decay rates (k'), obtained from the slopes of plots like the one shown in Fig. 6, are plotted as a function of [NO_x] in Fig. 7. The data suggest little or no pressure dependence in k_9 or k_{10} over the range 30–300 Torr. Combining data obtained at both pressures, the slopes of the k' versus [NO_x] plots give the following bimolecular rate coefficients (units are 10^{-11} cm^3 $molecule^{-1}$ s^{-1} and uncertainties are 2σ, precision only): $k_9 = 1.20 \pm 0.19$ and $k_{10} = 2.06 \pm 0.18$. Since side reactions appear to have little or no impact on the accuracy of reported rate coefficients, it appears that accuracy is limited primarily by precision and by the accuracy with which the concentrations of NO and NO_2 are known (estimated to be ±10% for each). Hence we report the following rate coefficients in units of 10^{-11} cm^3 $molecule^{-1}$ s^{-1}: $k_9 = 1.2 \pm 0.3$ and $k_{10} = 2.1 \pm 0.3$, where the uncertainties represent accuracy at the 95% confidence level.

3.6. Comparisons with the literature

All spectroscopic and kinetic parameters reported in this paper are new, i.e., there are no data in the literature that can be directly compared with our results. However, liquid phase data for $CH_3(Cl)S(O)CH_3$ are available in the literature [8–11], as are gas phase data for $(CH_3)_2S$–Cl [12] and $(CH_3)_2S$–Br [16,25]; hence, some interesting comparisons can be made.

Known spectroscopic properties of halogen atom adducts with DMSO and DMS (CH_3SCH_3) are summarized in Table 1. As mentioned above, the gas phase absorption spectrum of DMSO–Cl observed in this study is very similar to liquid phase spectra of DMSO–Cl that have been reported previously in both polar [11] and non-polar [8] solvents. The values of λ_{max} for DMS–Cl and DMS–Br are consistent with the normal trend that the spectrum of the bromine compound is red-shifted from the spectrum of the analogous chlorine compound. However, the substantial red-shift of the DMSO–Cl spectrum in comparison with the DMS–Cl spectrum is an interesting result that will require theoretical studies of the excited electronic states of these

Table 1
Spectroscopic properties of halogen atom adducts with $(CH_3)_2SO$ (DMSO) and $(CH_3)_2S$ (DMS)

Adduct	λ_{max}[a]	σ_{max}[a]	FWHM[a,b]	Reference
DMSO–Cl (l) (CCl_4 solvent)	399		6900	[8]
DMSO–Cl (l) (H_2O solvent)	389	2.2	6500	[11]
DMSO–Cl (g)	394	4.0	6500	This work
DMS–Cl (g)	340	3.4	5500	[12]
DMS–Br (g)	365	2.7	5900	[16]

[a] Units are λ_{max} (nm); σ_{max} (10^{-17} cm^2 $molecule^{-1}$, base e); FWHM (cm^{-1}).
[b] All spectral shapes are approximated by a Gaussian function when plotted as σ vs. λ. FWHM: full width at half maximum.

species to fully understand. All σ_{max} values listed in Table 1 are similar in magnitude and quite large. We have also observed peak absorption cross-sections of similar magnitude for the strongest transitions in the spectra of SCS–Cl [13] and RI–Cl (R = CH_3, C_2H_5) [26] (the spectra of these adducts show clear evidence for two electronic transitions). It seems that peak absorption cross-sections of order of magnitude 10^{-17} cm^2 $molecule^{-1}$ (base e) are characteristic of a variety of 2-center 3-electron bonded chromophores involving halogen atoms.

The rate coefficients obtained in this study for the reactions of DMSO–Cl with O_2, NO, and NO_2 are similar in magnitude to the analogous rate coefficients for DMS–Cl [12], SCS–Cl [13], and RI–Cl (R = CH_3, C_2H_5) [26]. In all cases, no observable reaction with O_2 is observed. On the other hand, all of the Cl adducts mentioned above react rapidly with NO and NO_2, with all rate coefficients falling in the range (1–4) × 10^{-11} cm^3 $molecule^{-1}$ s^{-1}. The observed reactivity trend is consistent with a Cl transfer mechanism. For the NO_x reactions, Cl transfer from the adduct to form the relatively stable compounds ClNO, $ClNO_2$, or ClONO is energetically favorable. On the other hand, the 298 K bond dissociation energy of Cl–OO is only ∼20 kJ mol^{-1} [27]. Since DMSO–Cl [6,7], DMS–Cl [7,28–32], SCS–Cl [33,34], CH_3I–Cl [35,36], and C_2H_5I–Cl [37] are all bound by more than 35 kJ mol^{-1}, Cl transfer from the adducts to O_2 cannot occur at room temperature and below.

The rate coefficient obtained in this study for the DMSO–Cl self-reaction is a factor of 2–8 slower than reported self-reaction rate coefficients for DMS–Cl [12], SCS–Cl [13], and RI–Cl [26], but appears to be faster than the reported self-reaction rate coefficient for DMS–Br [16]. Further research will be required to understand these differences in self-reaction reactivity.

3.7. Atmospheric chemistry of $CH_3(Cl)S(O)CH_3$

Concentrations of atomic chlorine are thought to be higher in the marine boundary layer (MBL) than in other parts of the troposphere. A recent estimate of the average Cl concentration in the MBL is ∼4 × 10^4 atoms cm^{-3} [38], i.e., about a factor of 20–25 smaller than the average tropospheric OH concentration (9 × 10^5 molecules cm^{-3} [39]). The two most important removal processes for atmospheric DMSO(g) are widely accepted to be gas phase reaction with OH and uptake into the condensed phase followed by condensed phase oxidation [1,40]. However, as discussed by Nicovich et al. [7], reaction with Cl could account for as much as 6% of DMSO loss in the MBL *if* loss of $CH_3(Cl)S(O)CH_3$ is dominated by processes that do not regenerate DMSO. The results reported in this paper taken in conjunction with the results reported by Nicovich et al. [7] allow us to examine the potential importance of the most likely tropospheric $CH_3(Cl)S(O)CH_3$ degradation pathways; these include photolysis, thermal dissociation, reaction with O_2, and reaction with NO_x.

The absorption cross-sections reported in this paper can be used in conjunction with tabulated actinic flux (F) data [41] and an assumed quantum yield of unity for $CH_3(Cl)S(O)CH_3$ destruction (the maximum and most probable value) to obtain a maximum first order $CH_3(Cl)S(O)CH_3$ photolysis rate, J_{max}:

$$J_{max}(\theta) = \int \sigma(\lambda) F(\lambda, \theta)\, d\lambda \qquad \text{(IV)}$$

The parameter θ in Eq. (IV) is the solar zenith angle. We obtain $J_{max} = 2.5\ s^{-1}$ at $\theta = 0^\circ$. At $\theta = 60^\circ$, which is close to the globally averaged zenith angle, J_{max} is reduced from the 0° value by approximately a factor of 2.

Temperature dependent rate coefficients for thermal dissociation of $CH_3(Cl)S(O)CH_3$ at atmospheric pressure can be estimated based on the kinetic and thermodynamic results reported by Nicovich et al. [7]. At temperatures of 260, 280, and 300 K the thermal dissociation rate coefficients are approximately 0.05 s^{-1}, 0.4 s^{-1}, and 3 s^{-1}, respectively.

Mixing ratios of NO_x in the remote MBL are only a few parts per trillion. Hence, reactions of $CH_3(Cl)S(O)CH_3$ with NO and NO_2 are potentially important only in relatively polluted coastal regions where NO_x mixing ratios can be in the parts per billion (ppb) range. For example, if one assumes 1 ppb NO_x (≈2.5 × 10^{10} molecules cm^{-3} at atmospheric pressure and typical lower atmospheric temperatures) and a rate coefficient of 1.6 × 10^{-11} cm^3 $molecule^{-1}$ s^{-1} for $CH_3(Cl)S(O)CH_3 + NO_x$ (based on this work), a first order rate coefficient of 0.4 s^{-1} is obtained for removal of $CH_3(Cl)S(O)CH_3$ by NO_x. Using the upper limit rate coefficient of 3 × 10^{-18} cm^3 $molecule^{-1}$ s^{-1} determined in this study for the $CH_3(Cl)S(O)CH_3 + O_2$ reaction leads to an upper limit first order rate coefficient of 15 s^{-1} for $CH_3(Cl)S(O)CH_3$ removal by O_2 at atmospheric pressure.

The analysis discussed above suggests that reaction with O_2 cannot be ruled out as the dominant removal process for $CH_3(Cl)S(O)CH_3$ in the troposphere. In the (probable) event that k_8 is actually much less than the upper limit value reported here, thermal dissociation is the dominant removal process at higher atmospheric temperatures while photolysis probably becomes dominant at lower temperatures. Reaction with NO_x may make a significant contribution to $CH_3(Cl)S(O)CH_3$ removal in polluted environments, particularly at lower temperatures. It is well established that thermal dissociation regenerates DMSO in high yield [7]. It is also quite likely that reaction with NO_x and photolysis produces DMSO in high yield, although additional experimental work to confirm these expectations would be welcome. Only if $k_8 > 10^{-19}$ cm^3 $molecule^{-1}$ s^{-1} or if photolysis results in high yields of products other than DMSO + Cl, will $CH_3(Cl)S(O)CH_3$ play a significant role in atmospheric chemistry.

Acknowledgments

This research was supported by the NSF Atmospheric Chemistry Program through grants ATM-9910912 and ATM-0350185. The participation of K.M. Kleissas was supported by a NSF-REU (Research Experiences for Undergraduates) grant to the School of Chemistry and Biochemistry of the Georgia Institute of Technology.

References

[1] I. Barnes, J. Hjorth, N. Mihalopoulos, Chem. Rev. 106 (2006) 940–975.

[2] I. Barnes, V. Bastian, K.H. Becker, D. Martin, Biogenic sulfur in the environment, in: E.S. Saltzman, W.J. Cooper (Eds.), ACS Symposium Series Number 393, American Chemical Society, Washington, DC, 1989, pp. 476–488.
[3] H. Falbe-Hansen, S. Sorensen, N.R. Jensen, T. Pedersen, J. Hjorth, Atmos. Environ. 34 (2000) 1543–1551.
[4] E. Martinez, A. Aranda, Y. Diaz de Mera, D. Rodriguez, M.R. Lopez, J. Albaladejo, Environ. Sci. Technol. 36 (2002) 1226–1230.
[5] V. Riffault, Y. Bedjanian, G. LeBras, Phys. Chem. Chem. Phys. 5 (2003) 2828–2835.
[6] S. Vandresen, S.M. Resende, J. Phys. Chem. A 108 (2004) 2284–2289.
[7] J.M. Nicovich, S. Parthasarathy, F.D. Pope, A.T. Pegus, M.L. McKee, P.H. Wine, J. Phys. Chem. A 110 (2006) 6874–6885.
[8] T. Sumiyoshi, M. Katayama, Chem. Lett. (1987) 1125–1126.
[9] K. Kishore, K.-D. Asmus, J. Phys. Chem. 95 (1991) 7233–7239.
[10] Z.B. Alfassi, S. Mosseri, P. Neta, J. Phys. Chem. 93 (1989) 1380–1385.
[11] L. Zhu, J.M. Nicovich, P.H. Wine, J. Phys. Chem. A 109 (2005) 3903–3911.
[12] S.P. Urbanski, P.H. Wine, J. Phys. Chem. A 103 (1999) 10935–10944.
[13] V. Dookwah-Roberts, R. Soller, J.M. Nicovich, P.H. Wine, J. Photochem. Photobiol. A: Chem. 176 (2005) 114–123.
[14] Z. Zhao, R.E. Stickel, P.H. Wine, Chem. Phys. Lett. 251 (1996) 59–66.
[15] A.J. Hynes, P.H. Wine, J. Atmos. Chem. 24 (1996) 23–37.
[16] T. Ingham, D. Bauer, R. Sander, P.J. Crutzen, J.N. Crowley, J. Phys. Chem. A 103 (1999) 7199–7209.
[17] T.B. Douglas, J. Am. Chem. Soc. 70 (1948) 2001–2002.
[18] E.G. Estupinan, J.M. Nicovich, P.H. Wine, J. Phys. Chem. A 105 (2001) 9697–9703.
[19] H. Okabe, J. Chem. Phys. 66 (1977) 2058–2062.
[20] C. Maul, T. Haas, K.-H. Gericke, J. Phys. Chem. A 101 (1997) 6619–6632.
[21] C. Maul, T. Haas, K.-H. Gericke, F.J. Comes, J. Chem. Phys. 102 (1995) 3238–3247.
[22] T. Einfeld, A. Chichinin, C. Maul, K.-H. Gericke, J. Chem. Phys. 116 (2002) 2803–2810.
[23] J.M. Nicovich, K.D. Kreutter, P.H. Wine, J. Chem. Phys. 92 (1990) 3539–3544.
[24] S.P. Sander, B.J. Finlayson-Pitts, R.R. Friedl, D.M. Golden, R.E. Huie, H. Keller-Rudek, C.E. Kolb, M.J. Kurylo, M.J. Molina, G.K. Moortgat, V.L. Orkin, A.R. Ravishankara, P.H. Wine, Chemical kinetics and photochemical data for use in atmospheric studies, Evaluation No. 15, JPL Publication 06-2, Jet Propulsion Laboratory, Pasadena, CA, 2006.
[25] P.H. Wine, J.M. Nicovich, R.E. Stickel, Z. Zhao, C.J. Shackelford, K.D. Kreutter, E.P. Daykin, S. Wang, The tropospheric chemistry of ozone in the polar regions, in: H. Niki, H. Becker (Eds.), NATO ASI Series, vol. I7, Springer-Verlag, Berlin Heidelberg, 1993, pp. 385–395.
[26] V. Dookwah-Roberts, J.M. Nicovich, P.H. Wine, 231st National Meeting of the American Chemical Society, Atlanta, GA, 2006, Paper PHYS 515.
[27] J.M. Nicovich, K.D. Kreutter, C.J. Shackelford, P.H. Wine, Chem. Phys. Lett. 179 (1990) 367–373, See for example.
[28] M.L. McKee, J. Phys. Chem. 97 (1993) 10971–10976.
[29] D.C. Young, M.L. McKee, in: J. Leszczynski (Ed.), Computational Chemistry: Reviews of Current Trends, vol. 4, World Scientific, Singapore, 1999, pp. 149–178.
[30] K.C. Thompson, C.E. Canosa-Mas, R.P. Wayne, Phys. Chem. Chem. Phys. 4 (2002) 4133–4139.
[31] S.M. Resende, W.B. De Almeida, J. Phys. Chem. A 101 (1997) 9738–9744.
[32] S. Enami, Y. Nakano, S. Hashimoto, M. Kawasaki, S. Aloisio, J.S. Francisco, J. Phys. Chem. A 108 (2004) 7785–7789.
[33] J.M. Nicovich, C.J. Shackelford, P.H. Wine, J. Phys. Chem. 94 (1990) 2896–2903.
[34] D. Wang, D.L. Phillips, Chem. Phys. Lett. 362 (2002) 205–209.
[35] Y.V. Ayhens, J.M. Nicovich, M.L. McKee, P.H. Wine, J. Phys. Chem. A 101 (1997) 9382–9390.
[36] S. Enami, S. Hashimoto, M. Kawasaki, Y. Nakono, T. Ishiwata, K. Tonokura, T.J. Wallington, J. Phys. Chem. A 109 (2005) 1587–1593.
[37] J.J. Orlando, C.A. Piety, J.M. Nicovich, M.L. McKee, P.H. Wine, J. Phys. Chem. A 109 (2005) 6659–6675.
[38] O.W. Wingenter, B.C. Sive, N.J. Blake, D.R. Blake, F.S. Rowland, J. Geophys. Res. 110 (2005) D20308, doi:10.1029/2005JD005875.
[39] R.G. Prinn, J. Huang, R.F. Weiss, D.M. Cunnold, P.J. Fraser, P.G. Simmonds, A. McCulloch, C. Harth, P. Salameh, S. O'Doherty, R.H. Wang, L. Porter, B.R. Miller, Science 292 (2001) 1882–1888.
[40] L. Zhu, A. Nenes, P.H. Wine, J.M. Nicovich, J. Geophys. Res. 111 (2006) D05316, doi:10.1029/2005/JD006326.
[41] B.J. Finlayson-Pitts, J.N. Pitts, Chemistry of the Upper and Lower Atmosphere, Academic Press, San Diego, 2000, See for example p. 66.